Sloppiness, robustness and evolvability in systems biology

Bryan C. Daniels, Yan-Jiun Chen, and James P. Sethna
Laboratory of Atomic and Solid State Physics, Cornell University, Ithaca, NY, USA

Ryan N. Gutenkunst
Department of Biological Statistics and Computational Biology, Cornell University, Ithaca, NY, USA

Christopher R. Myers
Computational Biology Service Unit, Life Sciences Core Laboratories Center, Cornell University, Ithaca, NY, USA

The functioning of many biochemical networks is often robust – remarkably stable under changes in external conditions and internal reaction parameters. Much recent work on robustness and evolvability has focused on the structure of neutral spaces, in which system behavior remains invariant to mutations. Recently we have shown that the collective behavior of multiparameter models is most often *sloppy*: insensitive to changes except along a few 'stiff' combinations of parameters, with an enormous sloppy neutral subspace. Robustness is often assumed to be an emergent evolved property, but the sloppiness natural to biochemical networks offers an alternative non-adaptive explanation. Conversely, ideas developed to study evolvability in robust systems can be usefully extended to characterize sloppy systems.

Introduction

Robustness and evolvability are major themes of systems biology, have been the subject of several recent books and reviews [1, 2, 3, 4, 5], and have been discussed alongside related phenomena such as canalization, homeostasis, stability, redundancy, and plasticity [6, 7, 8, 9]. Broadly construed, "robustness is the persistence of an organismal trait under perturbations" [5], which requires the specification of both traits of interest and perturbations under consideration. Recent work in systems biology has sought to distinguish between environmental robustness (e.g., temperature compensation in circadian rhythms [10, 11, 12]) and mutational robustness (e.g., parameter insensitivity in segment polarity patterning [13, 14]). Mutational robustness has a subtle relation to evolvability; while allowing survival under genetic alterations, robustness might seem to reduce the capacity for evolutionary adaptation on multigeneration time scales [4, 8].

Earlier robustness work focused on feedback and control mechanisms [15, 16, 17, 18, 19, 20]. Much recent work emphasizes neutral spaces and neutral networks: large regions in the space of sequences, parameters, or system topologies that give rise to equivalent (or nearly equivalent) phenotypic behaviors. Neutral spaces have been explored most extensively in the context of RNA secondary structure, where large neutral networks of RNA sequences (genotypes) fold into identical secondary structures (phenotypes) [8, 21, 22, 23]. More recently, similar ideas have been applied to neutral spaces underlying the robustness of gene regulatory networks [24, 25, 26], where different network topologies (genotypes) can result in identical gene expression patterns (phenotypes). Nontrivial niches in sequence spaces are also seen to emerge in molecular discrimination, a problem where neutral networks allow for biological communication in the presence of uncertainty akin to that found in engineered error-correcting codes [27]. Functional redundancies and degeneracies arise at many levels of biological organization [28], and it is an important open question as to how neutrality, redundancy, and robustness at different levels are organized and coupled across scales.

Despite these advances in understanding neutral networks connecting genotypes in discrete spaces (e.g., sequences), much of systems biology is focused on chemical kinetic networks that are parameterized by continuous parameter spaces. Often one is interested in the steady-state behavior of a dynamical system, or in the input-output response relating only a subset of the chemical species of a network. In principle, however, one must characterize the full dynamical behavior of a network, in part because any given network may be coupled in unknown ways to other subsystems that are not included in the model. To more clearly delineate distinct levels of biological organization, we have chosen to refer the space of continuous kinetic parameters as a "chemotype" [29], and to the full dynamical response of a system as its "dynatype" (Figure 1). The chemotype-to-dynatype maps of interest here are embedded within larger genotype-to-phenotype maps, with chemotypes emerging from lower-level processes, and dynatypes contributing to phenotypes and ultimately fitnesses on which selection acts. Recently, there has been increased interest in characterizing the parametric sensitivity of the dynamics of biochemical network models, for two important reasons: (1) to probe system robustness by quantifying the size and shape of chemotype spaces that leave system behavior unchanged, and (2) to characterize system behavior and uncertainties for which precise values for rate constants and other kinetic parameters are typically not known.

Parameter estimation in multiparameter models has long been known to be ill-conditioned: the collective be-

havior usually cannot be used to infer the underlying constants. Recent work has shown that these models share striking universal features [30, 31, 32, 33], a phenomenon that we have labeled "sloppiness" (see Figures 1 and 2). Sloppiness refers to the highly anisotropic structure of parameter space, wherein the behavior of models is highly sensitive to variation along a few 'stiff' directions (combinations of model parameters) and more or less insensitive to variation along a large number of 'sloppy' directions. A nonlinear least-squares cost function can be constructed:

$$C(\boldsymbol{\theta}) = \sum_i \frac{1}{2}\frac{(x(\boldsymbol{\theta}) - x_i)^2}{\sigma_i^2} = \sum_i \frac{1}{2} r_i^2, \qquad (1)$$

where $r_i = (x(\boldsymbol{\theta}) - x_i)/\sigma_i$ is the residual describing the deviation of a dynamical variable x from its measured values x_i with uncertainty σ_i. This cost reflects how well a model with a given set of parameters $\boldsymbol{\theta}$ fits observed experimental data. Parametric sensitivities of the model are encoded in the Jacobian matrix $J = \partial r_i/\partial\theta_j$. The curvature of the cost surface about a best fit set of parameters is described by the Hessian $H_{mn} = \partial^2 C/\partial\theta_m\theta_n$ (or its approximation, the Fisher Information Matrix $J^T J$). Stiff and sloppy directions are conveniently measured using an analysis of eigenvalues λ_n of the Hessian H (Figure 3); large eigenvalues correspond to stiff directions. For a broad range of multiparameter models (e.g., sixteen models drawn from the systems biology literature [32] and models from quantum Monte Carlo, radioactive decay, and polynomial fitting [34]) these eigenvalues are roughly uniformly spread over many decades, with many sloppy directions a thousand times less well determined than the stiffest, best constrained parameter combinations. Two consequences are that useful model predictions can be made even in the face of huge remaining parameter uncertainty, and conversely that direct measurements of the parameters can be inefficient in making more precise predictions [32]. Random matrix theory can be used to develop insight into the source of this type of eigenvalue spectrum and the nature of redundancies that appear to underly sloppiness [34]. Our open-source code SloppyCell (`http://sloppycell.sourceforge.net`) provides tools for exploring parameter space of systems biology models [35].

Others have recently addressed similar questions motivated by the lack of detailed information about kinetic parameters. These include: the inference of probabilistic statements about network dynamics from probability distributions on parameter values [36]; the use of "structural kinetic modeling" to parameterize the Jacobian matrix J and thereby probe ensembles of dynamical behaviors [37, 38]; the construction of convex parameter spaces ("k-cones") containing all allowable combinations of kinetic parameters for steady-state flux balance [39]; the use of ideas from control theory, worst-case analysis and hybrid optimization to measure the robustness of networks to simultaneous parameter variation [40], and exploration of correlated parameter uncertainties obtained via global inversion [41].

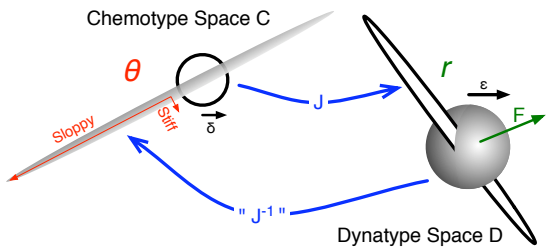

FIG. 1: **Sloppiness in the mapping of chemotypes to dynatypes.** It is natural, at least for cellular regulation and metabolic networks, to refine the traditional dichotomy of genotype G to phenotype P by adding two intermediate levels of description, $G \to C \to D \to P$. Here C is the *chemotype* [29], a continuous description of the behavior in terms of chemical reaction parameters (reaction rates, barriers and prefactors, or Michaelis-Menten parameters). D is the *dynatype*, meant to describe the dynamical responses of the cell (usually the time series of all species in response to selected stimuli, often taken from experimental measurements). Mutations about a particular chemotype $\boldsymbol{\theta}$ occupy a region in chemotype space (here a circle of radius δ), whose image in dynatype space is given by the local Jacobian J of the mapping: mutations along stiff directions in chemotype space will yield large changes in dynatype, while mutations along sloppy directions will lead to small dynamical changes. Conversely, a population of individuals sharing nearly the same dynatype $\mathbf{r}$ (here a sphere of radius ϵ) will occupy a distorted region in chemotype space, with large variations in reaction parameters possible along sloppy directions (gray ellipse).

Can we connect sloppiness to robustness and evolvability? It is our contention that sloppiness – the highly anisotropic structure of neutral variation in the space of chemotypes – has important implications for how one characterizes robustness in systems biology models. In addition, insights developed in the study of robustness and evolvability suggest new and potentially useful ways of analyzing and interpreting sloppiness.

Environmental robustness and sloppiness

Organisms must thrive under many environmental conditions: changing temperatures, salt concentrations, pH, nutrient densities, etc. Many organisms have explicit control mechanisms to keep their internal state insensitive to these external changes – these control mechanisms (homeostasis, adaptation, etc.) have been a historical focus in the robustness literature [15, 43]. For variations in temperature, however, many organisms do not have such homeostatic control (with the exception of birds, mammals, and some plants) and must instead cope with the exponential Arrhenius temperature dependence of all their reaction rates by some sort of compensatory mechanism [44].

The prototypical example of temperature compensa-

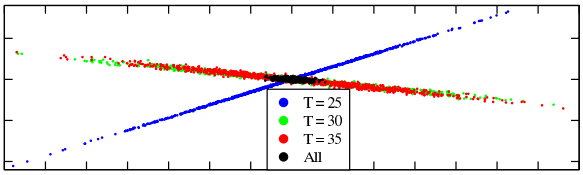

FIG. 2: **Sloppy parameter distributions: dependence on external conditions.** Shown is a two-dimensional view of the parameter sets (free energy barriers and prefactors) that accurately predict the experimental phosphorylation dynamics [11] in a 36-parameter subnetwork of a model of circadian rhythms [12], within a harmonic approximation (see Supplemental Material). Shown are parameters valid at three different temperatures (colors) and valid for all temperatures simultaneously (black). The plot shows one 'stiff' direction in parameter space for each temperature which is tightly constrained by the data, and one 'sloppy' direction which has relatively large variations without change in behavior. Most of the 34 other directions in parameter space not shown are sloppy; the two-dimensional view was chosen to best align with the stiffest direction for each of the four ensembles. The black region models organisms that are robust to temperature changes in this range. The acceptable region rotates and shifts with temperature, but the sloppiness allows different temperatures to intersect (robust temperature compensation) even though all rates are strongly temperature dependent.

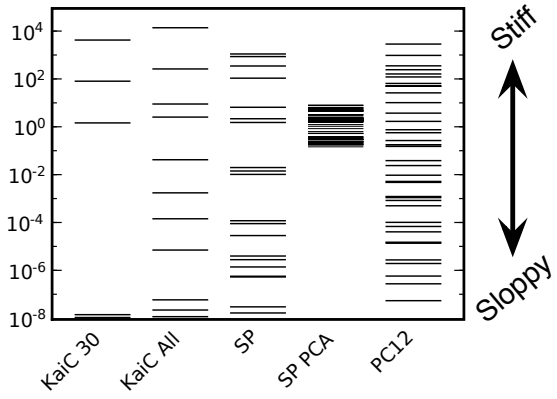

FIG. 3: **Sloppy model eigenvalues.** Shown are the eigenvalues of the approximate Hessian $J^T J$ for the goodness-of-fit $C(\boldsymbol{\theta})$ (Equation 1) about the best fit. Large eigenvalues correspond to stiff directions; others are sloppy. Notice the enormous range on this logarithmic scale; not all eigenvalues (ranging down to 10^{-20}) are depicted.

- Columns *KaiC 30* and *KaiC All* are for the KaiC phosphorylation dynamics model (Figure 3), showing $T = 30°$ C (yellow region in Figure 2) and simultaneous fits for all temperatures (black region). Notice that the 'robust' simultaneous fit has roughly one more stiff direction than the single temperatures.
- The *SP* and *SP PCA* columns are for the segment polarity model [13, 42]. *SP* is an eigenvalue analysis about one of the acceptable parameter sets, showing parameters that keep the behavior (dynatype) of the entire network preserved (time series for all components under all experimental conditions). *SP PCA* is a principal components analysis of the segment polarity ensemble that yields the wild-type phenotype, with parameters restricted to a relatively small range (roughly three decades each). Most directions in *SP* are sloppy enough to have fluctuations larger than the sampled phenotype box in *SP PCA*; the sloppy dynatype *SP* already explains the robustness to all but a few stiff directions in parameter space. Conversely, the sensitivity of the dynatype *SP* to a few stiff directions does not preclude phenotypic robustness in those directions for *SP PCA*; the dynatype (all dynamical evolution) is far more restrictive than the phenotype (output patterning).
- *PC12* is for the EGF/NGF growth-factor signaling network [31, 32]; note that it too is sloppy. See Figure 4 for an analysis of evolvability and robustness for this model.

tion is the 24-hour period of circadian rhythms [10]. Recent experiments have succeeded in replicating the circadian control network of cyanobacteria in the test tube using three Kai proteins, whose degree of phosphorylation oscillates with a temperature-compensated period in the range of 25 to 35° C. In addition, the phosphorylation dynamics of KaiC alone is found to be unchanged as the temperature varies in the same range [11]. This has been cited as a plausible explanation for the observed temperature compensation in the full network, presuming that all other rates are fast [12] and hence irrelevant to the period. (At least one other explanation of temperature compensation [45] also relies on constraining most rates to be irrelevant). Narrowing our focus to the KaiC phosphorylation subnetwork, however, still leaves the nontrivial task of explaining its temperature compensation mechanism, since estimated energy barriers [46] suggest that phosphorylation rates should be twice as fast at the higher temperature.

The dynamics of KaiC phosphorylation have been modeled using six phosphorylation sites and two conformational states (active and inactive) [12]. If each of the 18 rates in this model roughly double between 25 and 35°C, can we adjust the corresponding energy barriers and prefactors such that the resulting net phosphorylation dynamics is temperature-independent?

Figure 2 shows a two-dimensional view of the acceptable parameter sets in the resulting 36-dimensional space of energy barriers and prefactors, explored in the harmonic approximation (see Supplemental Material). Notice that the region of acceptable parameters rotates and shifts as the temperature changes. Notice also that the system is sloppy: Figure 2 shows one stiff direction that is highly constrained by the data and one sloppy direction that is largely unconstrained. The eigenvalue analysis in Figure 3 confirms that most directions in parameter space are sloppy and unconstrained. This provides a natural explanation for robustness: the intersection of these large, flat hypersurfaces yields parameters that work at all temperatures.[49] In general, each external condition provides one constraint per stiff direction; since there are only a few stiff directions and many parameters in sloppy models, robust behavior under varying external condi-

tions is easily arranged. Indeed, Figure 3 shows that the robust, temperature-independent fits for the KaiC model are themselves a sloppy system.

Chemotype robustness and sloppiness

In addition to robustness to environmental perturbation, biological networks are often robust to mutational perturbations; they maintain their function in the face of mutations that change one or perhaps more of their underlying rate parameters, and thus change their location in chemotype space. Some authors have used this as a criterion for judging model plausibility [47]. The quintessential example of a system that is chemotypically robust is the *Drosophila* segment polarity gene network. Early in development, this network generates a periodic macroscopic phenotype: a pattern of gene expression across several cells that persists throughout development and guides later stages. Multiparameter models of this network [13, 14, 47, 48] find that a surprisingly large fraction of randomly chose parameter sets generate a pattern consistent with the observed patterning of three genes – the system exhibits chemotype robustness.

In the context of sloppy models, we may define chemotype robustness as the fraction of a given volume in parameter/chemotype space C that maps into a functional region of behavior/dynatype space D (Figure 1). This latter functional region represents behavior close to optimum (or close to that measured experimentally). For simplicity, let us consider it to be a hypersphere of radius ϵ (i.e., a cost $C(\boldsymbol{\theta}) = \sum r_i^2/2 < \epsilon^2/2$ in Equation 1); larger changes in behavior are considered significantly different, perhaps lowering the organism's fitness. The given volume in chemotype space C might be (as for the segment polarity network) a hypercube of parameter ranges deemed reasonable, or (as a simple model of mutations) a hypersphere; let its scale be given by δ. Our robustness is therefore the fraction of all points in the δ-ball in C that map into the ϵ-ball in D – in Figure 1 the fraction of the circle whose interior is colored gray. This fraction can be calculated (see Supplemental Material) and is approximately given by

$$R_c = \prod_{\lambda_n > \lambda_{crit}} \sqrt{\frac{\lambda_{crit}}{\lambda_n}}, \tag{2}$$

where $\lambda_{crit} = \epsilon^2/\delta^2$. This formula can be motivated by considering the robust subregion (gray needle intersecting the circle) to be a slab, with thickness $\epsilon\sqrt{\lambda_n}$ along the eigendirection corresponding to each eigenvalue λ_n.[50] For sloppy directions with $\lambda_n < \epsilon^2/\delta^2 = \lambda_{crit}$, the slab is thicker than the circle and does not reduce the robust fraction; for each stiff direction with $\lambda_n > \lambda_{crit}$, the fractional volume is reduced roughly by a factor of the slab thickness $\epsilon\sqrt{\lambda_n}$ over the sphere width δ, leading to Equation (2).

In their model of segment polarity, von Dassow et al. found that approximately one in 200 randomly chosen parameter sets generated a wild-type expression pattern for three key genes [13]. This would naively seem amazing for a 48 parameter model like theirs; in an isotropic approximation, each parameter would be allowed only 6% chance of changing the wild-type pattern (since $0.94^{48} \sim 1/200$). However, we have previously shown that the segment polarity model is sloppy [32]. That is, going far beyond restricting the output phenotype, the dynamical evolution of every component of the network is approximately preserved even with huge changes in parameter values: only a few stiff directions in chemotype space are needed to maintain the dynatype (see column *SP* in Figure 3). Sloppiness hence provides a natural explanation for the wide variations in all but a few directions in parameter space.

The success rate of one in 200 is not nearly as striking if the dynamics is already known to be insensitive to all but perhaps four or five combinations of parameters: $0.35^5 \times 1^{43} \sim 1/200$. Column *SP PCA* in Figure 3 fleshes this picture out with a principal components analysis (PCA) of the robust region seen in von Dassow et al.'s original model, reconstructed using Ingeneue [42]. Note that these PCA eigenvalues are cut off from below by the parameter ranges chosen by the original authors for exploration (typically three decades per parameter). While the overall scale of the dynatype sloppy-model eigenvalues in *SP* and the phenotype eigenvalues in *SP PCA* cannot be directly compared, it is clear that the vast majority of sloppy-model eigenvalues are too small to constrain the parameters within the explored region. The model is robust in these directions not because of evolution and fitness, but because the dynamics of chemical reaction networks is mathematically naturally dependent only on a few combinations of reaction parameters.

Robustness, evolvability, and sloppiness

Mutational robustness of systems would seem to be at odds with an ability to adapt and evolve, since robustness implies persistence of phenotype or function, which may inhibit the capacity for evolutionary change. The concept of neutral spaces has been used – most notably by Wagner and collaborators – to suggest a resolution of this apparent paradox, as demonstrated in model systems exploring various genotype-to-phenotype maps [8, 23, 24, 25]. The important insight is that neutral spaces and neutral networks enable systems to drift robustly in genotype space (i.e., without significant phenotypic change), while encountering new and different phenotypes at various points along that neutral space. This insight results from a distinction between the robustness and evolvability of any given genotype, and the robustness and evolvability of all genotypes consistent with a given phenotype [8].

Evolvability is postulated to reflect the range of possi-

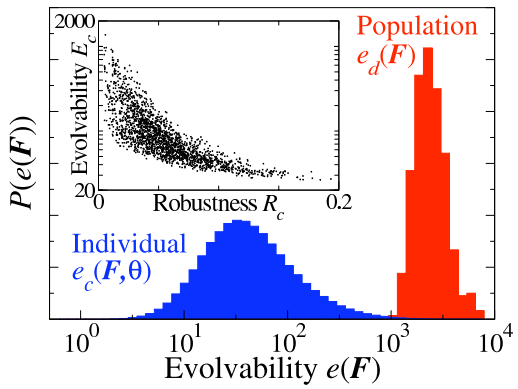

FIG. 4: **Evolvability and robustness in a sloppy system.** Evolvability distributions, and evolvability versus robustness, for an ensemble of parameters for a model of an EGF/NGF signaling pathway fitted to experimental data in PC12 cells [32]. The histogram on the left is the distribution of individual/chemotype evolvabilities $e_c(\mathbf{F}, \boldsymbol{\theta}_\alpha)$ (Equation 3), as $\mathbf{F}$ (an evolutionary pressure in dynatype space) is randomly chosen in direction with uniform magnitude and $\boldsymbol{\theta}_\alpha$ varies over the ensemble. The histogram on the right is the corresponding distribution of population/dynatype evolvabilities $e_d(\mathbf{F})$ (Equation 4). Note that the population evolvabilities are significantly higher than the individual ones. The inset plots the RMS individual chemotype evolvability $E_c(\boldsymbol{\theta}_\alpha)$ versus the robustness $R_c(\boldsymbol{\theta}_\alpha)$ (Equation 2) for the ensemble. (λ_{crit} is chosen as the fourth-stiffest eigenvalue at the best fit: see Supplemental Material). Note that, for each individual, more robustness leads to less evolvability – individuals which rarely mutate to new forms can't evolve as readily. This need not apply to the population, insofar as we expect robust dynatypes to explore larger regions of parameter/chemotype space, and thus the ratio of dynatype to chemotype evolvability to increase with increasing robustness.

ble different phenotypes that are possible under genotypic mutation. How does the sloppy connection between parameters and behavior impinge on the question of evolvability? Translating previous work on discrete genotype and phenotype spaces to the continuous spaces of chemotypes and dynatypes is nontrivial. Since the dimensionality of the space of chemotypes is less than that of dynatypes, the volume of dynatype space accessible under changes in chemotype is zero, i.e., lies on a lower-dimensional subspace. To develop a sensible definition of evolvability in such systems, we postulate forces $\mathbf{F}$ in dynatype space (Figure 1) that reflect evolutionary pressures due to changes in the environment, such that a change $\mathbf{r}$ in dynatype leads to a change $\mathbf{r} \cdot \mathbf{F}$ in fitness. An organism's evolvability is related to its capacity to respond to external forces through appropriate mutations in chemotype.

For a given force $\mathbf{F}$, the maximum fitness change among mutations of size δ in chemotype space is given by:

$$e_c(\mathbf{F}, \boldsymbol{\theta}) = \sqrt{\mathbf{F}^T J J^T \mathbf{F}}\, \delta \tag{3}$$

which we call the chemotype evolvability distribution (see Supplemental Material). Refs. [31] and [32] generate ensembles of parameters (chemotypes) consistent with a given dynatype for an EGF/NGF signaling pathway in PC12 cells, where the dynatype is constrained to fit available experimental data. (The PC12 network is sloppy, see Figure 3.) Each member of such an ensemble $\boldsymbol{\theta}_\alpha$ has a Jacobian J_α. As in Ref. [8], which distinguishes between genotype and phenotype evolvability, we can distinguish between the chemotype $e_c(\mathbf{F}, \boldsymbol{\theta}_\alpha)$ and dynatype

$$e_d(\mathbf{F}) = \max_{\theta_\alpha} e_c(\mathbf{F}, \boldsymbol{\theta}_\alpha) \tag{4}$$

evolvability distributions. The first gives the distribution of adaptive responses to $\mathbf{F}$ of individual chemotypes in a population, while the second gives the optimal response within the population. Figure 4 shows the chemotype and dynatype evolvability distributions, generated using the PC12 ensemble of Ref. [32] and a uniform distribution of force directions $\mathbf{F}$ in dynatype space. Within a population sharing the same behavior, we find substantial variation of accessible behavior changes, leading to a substantially larger population (dynatype) evolvability than individual (chemotype) evolvability. This echoes the finding of Wagner that phenotype evolvability is greater than genotype evolvability for RNA secondary structures [8].

It is natural to define an overall evolvability as the root-mean-square average of the evolvability distribution over a spherical distribution of environmental forces $\mathbf{F}$ in dynatype space:

$$E_c(\boldsymbol{\theta}_\alpha) = \sqrt{\langle (e_c(\mathbf{F}, \boldsymbol{\theta}_\alpha)^2 \rangle_{\mathbf{F}}} \tag{5}$$

and correspondingly for the overall RMS dynatype evolvability. The inset to Figure 4 shows that the chemotype evolvability decreases as the chemotype robustness increases, closely analogous to Wagner's discovery that genotype evolvability decreases as genotype robustness increases, except that his plot averages over phenotypes while ours represents variation within a dynatype. Thus we reproduce Wagner's observation [8] that individual evolvability decreases with robustness and that population evolvability is significantly larger than individual evolvability.[51]

Conclusion

Our previous work aimed at developing predictive systems biology models in the face of parametric uncertainty has led us to formulate a theory of sloppiness in multiparameter models. The picture that emerges from this theory is of a highly anisotropic neutral space in which variation in parameters (chemotypes) can leave system

behavior (dynatypes) unchanged. This picture is reminiscent in many ways to the notion of neutral spaces and neutral networks that has been developed to explore the robustness and evolvability of biological systems. We have been motivated by those ideas to here reconsider sloppiness within that context, both to highlight implications of sloppiness for the study of robustness and evolvability, and to identify new methods for analyzing sloppy systems.

Acknowledgments

We would like to thank Ben Machta and Mark Transtrum for their keen insights into sloppiness and their assistance in developing some of the arguments presented here. We acknowledge grants USDA-ARS 1907-21000-027-03, NSF DMR-070167, and NSF DGE-0333366.

References and recommended reading

1. Wagner A: *Robustness and Evolvability in Living Systems*. Princeton University Press; 2005.
2. de Visser JAGM, Hermisson J, Wagner GP, Meyers LA, Bagheri-Chaichian H, Blanchard JL, Chao L, Cheverud JM, Elena SF, Fontana W, et al.: **Perspective: Evolution and detection of genetic robustness**. *Evolution* 2003, **57**:1959–1972.
3. Jen E (Ed.): *Robust Design: A Repertoire of Biological, Ecological, and Engineering Case Studies*. Santa Fe Institute Studies in the Sciences of Complexity. Oxford University Press; 2005.
4. Lenski RE, Barrick JE, Ofria C: **Balancing robustness and evolvability**. *PLoS Biol* 2006, **4**:e428.
5. Felix MA, Wagner A: **Robustness and evolution: concepts, insights and challenges from a developmental model system**. *Heredity* 2008, **100**:132–140.
6. Kitano H: **Towards a theory of biological robustness**. *Mol Syst Biol* 2007, **3**:137.
7. Jen E: **Stable or robust? What's the difference?** *Complexity* 2003, **8**:12–18.
8. Wagner A: **Robustness and evolvability: a paradox resolved**. *Proc R Soc Lond B Biol Sci* 2008, **275**:91–100.
   •• Introduces the notion of phenotype robustness and phenotype evolvability in which the apparent tension between robustness and evolvability is resolved, and applies these ideas to the study of RNA secondary structures.
9. Krakauer D, Plotkin J: **Principles and parameters of molecular robustness**. In *Robust Design: A Repertoire of Biological, Ecological, and Engineering Case Studies*, edited by Jen E, Oxford University Press; 2005: 71–104.
10. Pittendrigh CS: **On temperature independence in the clock system controlling emergence time in Drosophila**. *Proc Natl Acad Sci U S A* 1954, **40**:1018–1029.
11. Tomita J, Nakajima M, Kondo T, Iwasaki H: **No transcription-translation feedback in circadian rhythm of KaiC phosphorylation**. *Science* 2005, **307**:251–254.
12. van Zon JS, Lubensky DK, Altena PRH, ten Wolde PR: **An allosteric model of circadian KaiC phosphorylation**. *Proc Natl Acad Sci U S A* 2007, **104**:7420–7425.
   • Presents a model of circadian rhythms in cyanobacteria, from which we extracted the submodel for KaiC phosphorylation dynamics.
13. von Dassow G, Meir E, Munro EM, Odell GM: **The segment polarity network is a robust developmental module**. *Nature* 2000, **406**:188–192.
14. Chaves M, Sontag ED, Sengupta AM: **Shape, size and robustness: feasible regions in the parameter space of biochemical networks** 2007. URL `http://arXiv.org/abs/0710.4269`.
15. Barkai N, Leibler S: **Robustness in simple biochemical networks**. *Nature* 1997, **387**:913–917.
16. Alon U, Surette MG, Barkai N, Leibler S: **Robustness in bacterial chemotaxis**. *Nature* 1999, **397**:168–171.
17. Yi TM, Huang Y, Simon MI, Doyle J: **Robust perfect adaptation in bacterial chemotaxis through integral feedback control**. *Proc Natl Acad Sci U S A* 2000, **97**:4649–4653.
18. Doyle J, Csete M: **Motifs, control, and stability**. *PLoS Biol* 2005, **3**:e392.
19. Goulian M: **Robust control in bacterial regulatory circuits**. *Curr Opin Microbiol* 2004, **7**:198–202.
20. Kurata H, El-Samad H, Iwasaki R, Ohtake H, Doyle JC, Grigorova I, Gross CA, Khammash M: **Module-based analysis of robustness tradeoffs in the heat shock response system**. *PLoS Comput Biol* 2006, **2**:e59.
21. Schuster P, Fontana W: **Chance and necessity in evolution: lessons from rna**. *Physica D* 1999, **133**:427–452.
22. Fontana W: **Modelling 'evo-devo' with RNA**. *Bioessays* 2002, **24**:1164–1177.
23. Sumedha, Martin OC, Wagner A: **New structural variation in evolutionary searches of RNA neutral networks**. *Biosystems* 2007, **90**:475–485.
24. Ciliberti S, Martin OC, Wagner A: **Robustness can evolve gradually in complex regulatory gene networks with varying topology**. *PLoS Comput Biol* 2007, **3**:e15.
25. Ciliberti S, Martin OC, Wagner A: **Innovation and robustness in complex regulatory gene networks**. *Proc Natl Acad Sci U S A* 2007, **104**:13591–13596.
   • Examines the structure of neutral networks and connections between robustness and evolvability in a simple model of gene regulatory networks.
26. Bergman A, Siegal ML: **Evolutionary capacitance as a general feature of complex gene networks**. *Nature* 2003, **424**:549–552.
27. Myers CR: **Satisfiability, sequence niches, and molecular codes in cellular signaling** 2007. URL `http://arXiv.org/abs/q-bio/0702042`.
   • Explores the nontrivial structure of neutral spaces that arise from the satisfaction of conflicting constraints in a genotype-to-phenotype map relating protein sequences to the avoidance of crosstalk.
28. Edelman GM, Gally JA: **Degeneracy and complexity in biological systems**. *Proc Natl Acad Sci U S A* 2001, **98**:13763–13768.
29. Gutenkunst RN, Sethna JP: **Adaptive mutation in a geometrical model of chemotype evolution** 2007. URL `http://arXiv.org/abs/0712.3240`.
30. Brown KS, Sethna JP: **Statistical mechanical ap-**

proaches to models with many poorly known parameters. *Phys Rev E* 2003, **68**:021904.

31. Brown KS, Hill CC, Calero GA, Myers CR, Lee KH, Sethna JP, Cerione RA: **The statistical mechanics of complex signaling networks: nerve growth factor signaling**. *Phys Biol* 2004, **1**:184.
32. Gutenkunst RN, Waterfall JJ, Casey FP, Brown KS, Myers CR, Sethna JP: **Universally sloppy parameter sensitivities in systems biology models**. *PLoS Comput Biol* 2007, **3**:e189.
    •• Demonstrates the universality of sloppy eigenvalue spectra in chemical kinetic network models from systems biology, and highlights the inefficiency of constraining models by direct parameter measurement because of this sloppy structure.
33. Gutenkunst RN, Casey FP, Waterfall JJ, Myers CR, Sethna JP: **Extracting falsifiable predictions from sloppy models**. *Ann NY Acad Sci* 2007, **1115**:203–211.
34. Waterfall JJ, Casey FP, Gutenkunst RN, Brown KS, Myers CR, Brouwer PW, Elser V, Sethna JP: **Sloppy-model universality class and the Vandermonde matrix**. *Phys Rev Lett* 2006, **97**:150601.
    • Discusses the mathematical origins of sloppy behavior in multiparameter models, with examples of sloppy model behavior outside of biology.
35. Myers CR, Gutenkunst RN, Sethna JP: **Python unleashed on systems biology**. *Comput Sci Eng* 2007, **9**:34–37.
36. Liebermeister W, Klipp E: **Biochemical networks with uncertain parameters**. *IEE P Syst Biol* 2005, **152**:97–107.
37. Steuer R, Gross T, Selbig J, Blasius B: **Structural kinetic modeling of metabolic networks**. *Proc Natl Acad Sci U S A* 2006, **103**:11868–11873.
38. Grimbs S, Selbig J, Bulik S, Holzhutter HG, Steuer R: **The stability and robustness of metabolic states: identifying stabilizing sites in metabolic networks**. *Mol Syst Biol* 2007, **3**:146.
39. Famili I, Mahadevan R, Palsson BO: **k-cone analysis: Determining all candidate values for kinetic parameters on a network scale**. *Biophys J* 2005, **88**:1616–1625.
40. Kim J, Bates DG, Postlethwaite I, Ma L, Iglesias PA: **Robustness analysis of biochemical network models**. *IEE P Syst Biol* 2006, **153**:96–104.
41. Piazza M, Feng XJ, Rabinowitz JD, Rabitz H: **Diverse metabolic model parameters generate similar methionine cycle dynamics**. *J Theor Biol* 2008, **251**:628–639.
42. Meir E, Munro EM, Odell GM, Dassow GV: **Ingeneue: A versatile tool for reconstituting genetic networks, with examples from the segment polarity network**. *J Exp Zool* 2002, **294**:216–251.
43. Stelling J, Sauer U, Szallasi Z, Doyle FJ, Doyle J: **Robustness of cellular functions**. *Cell* 2004, **118**:675–685.
44. Ruoff P, Rensing L, Kommedal R, Mohsenzadeh S: **Modeling temperature compensation in chemical and biological oscillators**. *Chronobiol Int* 1997, **14**:499–510.
45. Hong CI, Conrad ED, Tyson JJ: **A proposal for robust temperature compensation of circadian rhythms**. *Proc Natl Acad Sci U S A* 2007, **104**:1195–1200.
46. Cheng Y, Zhang Y, McCammon JA: **How does activation loop phosphorylation modulate catalytic activity in the cAMP-dependent protein kinase: A theoretical study**. *Protein Sci* 2006, **15**:672–683.
47. Ma W, Lai L, Ouyang Q, Tang C: **Robustness and modular design of the Drosophila segment polarity network**. *Mol Syst Biol* 2006, **2**:70.
48. Ingolia NT: **Topology and robustness in the Drosophila segment polarity network.** *PLoS Biol* 2004, **2**:e123.
49. In the particular case of KaiC, we find that successful chemotypes favor dephosphorylation in the active state and phosphorylation in the inactive state (see Supplemental Material), so the thermally robust solutions presumably increase the proportion of protein in the inactive state as temperature increases, compensating for the general speedup of all rates.
50. The cost for a small displacement of size $\Delta\theta$ along the eigendirection n is $\lambda_n \Delta\theta^2/2$, which equals $\epsilon^2/2$ when $\Delta\theta = \pm\epsilon\sqrt{\lambda_n}$.
51. Unfortunately, we cannot reproduce Wagner's final conclusion (that phenotype evolvability increases with phenotype robustness), since our ensemble (generated to match experimental behavior) is confined to the single PC12 species (dynatype).

Supplemental Material

Sloppiness, robustness, and evolvability in systems biology

Bryan C. Daniels, Yan-Jiun Chen, James P. Sethna, Ryan N. Gutenkunst, and Christopher R. Myers

Contents

The contents of the supplemental material are organized corresponding to the order of the main text. Included in the supplemental material are derivations of mathematical results and details of the specific models mentioned in the main text.

We have also posted the data files and computer codes for the models discussed, at `http://www.lassp.cornell.edu/sethna/Sloppy`. For the KaiC, PC12, and segment polarity models, this includes:

1. Equations in LaTeX, Python, and C
2. SBML (system biology markup language) files
3. Parameter ensembles
4. Best-fit Hessian and J^TJ, and their eigenvectors and eigenvalues

Introduction

Hessian at best fit parameters

In the introduction we mention that "the curvature of the cost surface about a best fit set of parameters is described by the Hessian H_{mn}." Examining the behavior of H_{mn} is a standard method for nonlinear least squares models when fitting data. Formally, H_{mn} is written as:

$$H_{mn} = \frac{\partial^2 C}{\partial\theta_m\theta_n} = \sum_i \frac{\partial r_i}{\partial\theta_m}\frac{\partial r_i}{\partial\theta_n} + r_i\frac{\partial^2 r_i}{\partial\theta_m\theta_n}. \qquad \text{(S1)}$$

If the model fits the data well so that $r_i \approx 0$ (or perfectly, Ref. [32] in the main text) then

$$H_{mn}(\boldsymbol{\theta}^*) \approx \sum_i \frac{\partial r_i}{\partial\theta_m}\frac{\partial r_i}{\partial\theta_n} = (J^TJ)_{mn}. \qquad \text{(S2)}$$

If H and the cost are used (as in this review) to describe changes in model behavior from $\boldsymbol{\theta}^*$, then $\mathbf{r} \equiv 0$ at $\boldsymbol{\theta}^*$ and Equation (S2) is exact. Notice also that H reflects the sensitivity of the fit to changes in parameters; in fact, its inverse is the covariance matrix. The diagonal elements of the covariance matrix are proportional to the uncertainties in the parameters, while the off-diagonal elements are estimates of parameter uncertainty correlations.

Figure 1: Sloppiness in the mapping of chemotypes to dynatypes

Shown in Figure 1 of the main text is the mapping of chemotypes C to dynatypes D. The mapping between C and D is described with J and "J^{-1}". It is typical that $\dim(C) \ll \dim(D)$, since there are typically more data points constraining the dynatype than there are parameters defining a chemotype. Therefore, the inverse of J is not well-defined. In Figure 1, the gray ellipse in C represents the inverse image of the ϵ-ball, B_ϵ, in D under J. That is, "J^{-1}" acting on B_ϵ is the set $\{\mathbf{c} \in C \ s.t. \ J\cdot\mathbf{c} \in B_\epsilon\}$.

Note also that the stiff and sloppy eigendirections in C and their images in D can be described by the singular value decomposition of the Jacobian J. Since λ_n are eigenvalues of J^TJ, $\sqrt{\lambda_n}$ are the singular values of J. Furthermore, writing $J = U\sum V^T$, we see that the columns of V are stiff/sloppy eigenparameters in C (shown in red in the figure), and the columns of U are images of stiff and sloppy eigenparameters (divided by λ_n) in D.

Environmental robustness and sloppiness

Figure 2: Sloppy parameter distributions: dependence on external conditions

In Figure 2 of the main text, the plane onto which the ensembles are projected is the one that aligns best with the stiffest eigenparameter of each of the four ensembles. To accomplish this, the vertical and horizontal axes in Figure 2 are, respectively, the first and second singular vectors in the singular value decomposition of the set of stiffest eigenparameters $\{\mathbf{v}_0^{25}, \mathbf{v}_0^{30}, \mathbf{v}_0^{35}, \mathbf{v}_0^{All}\}$. In a way analogous to principal components analysis, this gives the plane that passes through the origin and comes closest to passing through the heads of unit vectors pointing in the stiffest eigendirections.

Each ensemble of parameter sets shown in Figure 2 is chosen from the probability distribution corresponding to the local quadratic approximation of the cost near the best-fit parameters $\boldsymbol{\theta}^*$:

$$P(\boldsymbol{\theta}^* + \Delta\boldsymbol{\theta}) \propto \exp(-\Delta\boldsymbol{\theta}J^TJ\Delta\boldsymbol{\theta}/2). \qquad \text{(S3)}$$

This local approximation to the cost was used to generate the ensembles instead of the full nonlinear cost function due to difficulties in generating equilibrated ensembles: the thin curving manifolds of allowable chemotypes for sloppy models can be notoriously difficult to populate. But this is not impossible; efforts are still underway, and if equilibrated ensembles are found, they will be posted to the website mentioned above.

KaiC phosphorylation subnetwork model

In the main text, we use as an example a portion of the circadian rhythm model presented in Ref. [12] of the

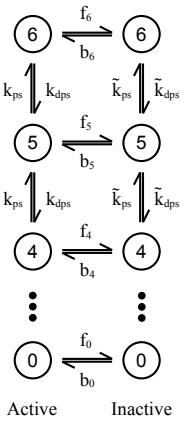

FIG. S1: **KaiC phosphorylation subnetwork.** This schematic depicts the KaiC network used as an example in the main text. It is a portion of the full circadian rhythm model presented in Ref. [12] of the main text. The numbers represent the degree of phosphorylation, and the two columns represent two different conformational states, "active" and "inactive." The labels on the arrows represent reaction rates for changing among the phosphorylation and conformation states. Each conformation state has one phosphorylation and one dephosphorylation rate, independent of the degree of phosphorylation. Each of the 14 "flip" rates between conformational states (b_i and f_i) is allowed to vary independently. This gives a total of 18 reaction rates.

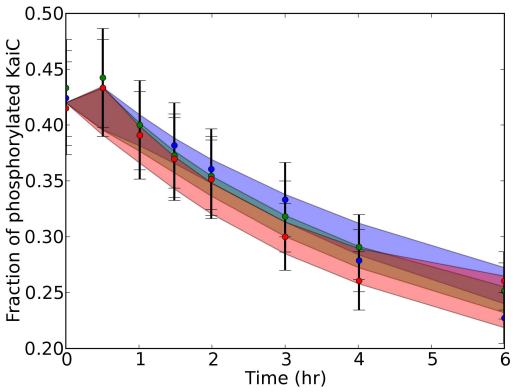

FIG. S2: **KaiC phosphorylation network: temperature-compensated output.** Shown is the net phosphorylation of KaiC over time, comparing experimental data (circles with error bars, from Ref. [11] in the main text) with output from an ensemble of chemotypes (filled colored regions, showing the mean plus or minus one standard deviation over the ensemble for the net phosphorylation at each time-point). Different colors correspond to different temperatures: blue = 25°, green = 30°, red = 35°. Note that the chemotypes describe the data well at all three temperatures, even though the rates are strongly dependent on temperature.

main text. We implement the subnetwork that van Zon et al. hypothesize must have intrinsically temperature-independent rates: that which controls the phosphorylation of KaiC alone. This subnetwork models the experimental measurements of KaiC phosphorylation in the absence of KaiA and KaiB (Ref. [11] of the main text), in which the phosphorylation of KaiC does not oscillate, but decays at a temperature-compensated rate in the range from 25 to 35° C (see circles in Figure S2).

The subnetwork involves an active and inactive state of KaiC, along with six phosphorylation sites for each state, as depicted in Figure S1. Including forward and backward "flip" rates between active and inactive states along with (de)phosphorylation rates that are each constant for the two states, there are 18 independent rates. To assess the temperature dependence, we assume that each transition rate follows an Arrhenius law, with constant energy barrier E and prefactor α: the ith rate is $\alpha_i e^{E_i/kT}$. This then gives a 36-dimensional chemotype space in which to search for solutions.

Temperature-independent solutions can be trivially found in this space if the energy barriers are chosen to be small, since this produces rates that are inherently weakly dependent on temperature. In order to avoid this trivial temperature compensation, we apply a prior that favors solutions with phosphorylation energy barriers near the expected $E_0 = 23\ kT$, similar to those found in other kinases (Ref. [46] in the main text) and appropriate for reactions that break covalent bonds. We choose this prior as a quartic in $\log E$:

$$C_{prior} = \frac{25}{2}\left[\log\left(\frac{E}{E_0}\right)\right]^4. \tag{S4}$$

The form was chosen to severely penalize barriers less than 10 kT, but to be reasonably flat around E_0; other prior choices would presumably perform similarly.

Using this method, we find that it is possible to fit the experimental data even with (de)phosphorylation rates that are strongly temperature-dependent. The phosphorylation and dephosphorylation rates that provided a best fit to all temperatures simultaneously were all above 21 kT. We used Bayesian Monte-Carlo sampling of chemotype space to create an ensemble of parameter sets that each produce phosphorylation dynamics that match the experimental data at 25, 30, and 35° C. As explained above, our ensemble has not yet sampled all the space available, but we still find many such acceptable chemotypes. The minimum (de)phosphorylation rate for the ensemble was just under 10 kT, so the prior worked as designed to confine the barriers to physically reasonable values. Figure S2 shows the output of the model over this ensemble of parameter sets compared with the experimental data from Ref. [11] of the main text.

We mention in a footnote that, in our model, "successful chemotypes favor dephosphorylation in the active state and phosphorylation in the inactive state." This can be seen in the ratio of phosphorylation to dephosphorylation rates, shown in Figure S3, for the ensemble of successful chemotypes. Note that most members of the

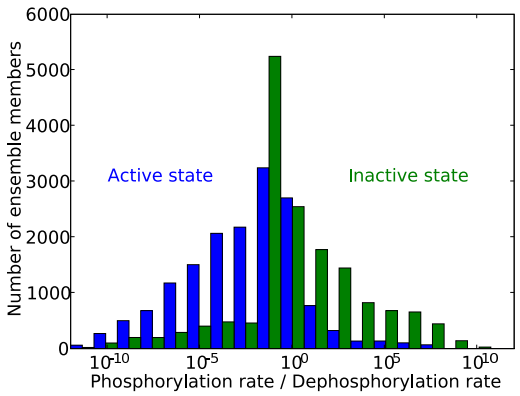

FIG. S3: **KaiC phosphorylation network: temperature-compensation mechanism.** This plot shows the ratios of phosphorylation rates to dephosphorylation rates for the active and inactive states – the distribution of k_{ps}/k_{dps} is shown in blue for the active state, and the distribution of $\tilde{k}_{ps}/\tilde{k}_{dps}$ is shown in green for the inactive state (see Figure S1 for definitions of rate constants). The distribution is over the same (non-equilibrated) ensemble as was used to generate Figure S2. Note that phosphorylation is favored in the inactive state, while dephosphorylation is favored in the active state. This suggests a temperature-compensation mechanism, as described in the text.

ensemble have an inactive state with higher phosphorylation rate than dephosphorylation, and vice versa for the active state. This matches with an intuitive temperature-compensation mechanism: with flip rates that are also temperature-dependent, higher temperatures can lead to more KaiC being in the inactive state, leading to a slower overall decay in phosphorylation that compensates for the speedup in reaction rates.

Figure 3: Sloppy model eigenvalues

The PCA shown in Figure 3 column *SP PCA* was produced after taking logarithms of the parameter values that von Dassow *et al.* used in their analysis. This measures parameter fluctuations in terms of fractional changes in parameter, rather than absolute sizes of fluctuations – allowing fluctuations in parameters with different units, for example, to be compared. The parameters used in column *SP* were chosen (logarithmic or otherwise) as defined by the original authors. Taking logarithms and/or changing units does not typically change the qualitative spectra of sloppy models, as their spectra already span so many decades.

Chemotype robustness and sloppiness

Derivation of robustness equation

In the main text (MT), the robustness is defined as

$$R_c = \prod_{\lambda_n > \lambda_{crit}} \sqrt{\frac{\lambda_{crit}}{\lambda_n}}. \qquad \text{(MT 2)}$$

We now proceed to derive this result. We measure robustness as the fraction of mutations of a given size δ in C (chemotype space) that do not change the behavior beyond a given threshold (survival after a mutation), which we designate as an ϵ-ball around the optimum in D (dynatype space). Therefore we want an estimate of the fraction of the δ-ball in C that maps into the ϵ-ball in D. It is difficult to calculate this geometrically, since we would need to find the volume of an ellipsoid intersecting a sphere. Fortunately, for sloppy systems, the λ_i vary over many orders of magnitude, so we can simplify the calculation by smearing the δ-ball and ϵ-ball into Gaussians. Namely, we say a mutation $\Delta\boldsymbol{\theta}$ in C has probability $e^{-(\Delta\boldsymbol{\theta})^2/2\delta^2}/(\sqrt{2\pi}\delta)^N$, and the probability of "survival" in D is given by $e^{-r^2/2\epsilon^2}$. We then measure the robustness as the overall probability $P(\delta,\epsilon)$ of surviving after a mutation:

$$\begin{aligned} R_c &= P(\delta,\epsilon) \\ &= \left(\frac{1}{\sqrt{2\pi}\delta}\right)^N \int_C \mathrm{d}\Delta\boldsymbol{\theta}\, \exp(-(\Delta\boldsymbol{\theta})^2/2\delta^2) \exp(-(\Delta\boldsymbol{\theta})^T J^T J(\Delta\boldsymbol{\theta})/2\epsilon^2) \\ &= \prod_n \frac{1}{\sqrt{1+\lambda_n\,\delta^2/\epsilon^2}}. \end{aligned} \qquad \text{(S5)}$$

For sloppy systems, λ varies over many orders of magnitude. Notice that if $\lambda_n \ll \epsilon^2/\delta^2$, its component in the product will be close to 1, and if $\lambda_n \gg \epsilon^2/\delta^2$, we can approximate the components in the product as $\sqrt{\epsilon^2/\delta^2\lambda_n}$. Therefore, using our definition $\lambda_{crit} \equiv \epsilon^2/\delta^2$ we can ap-

proximate this formula as:

$$R_c \approx \prod_{\lambda_n > \epsilon^2/\delta^2} \sqrt{\frac{\epsilon^2}{\delta^2 \lambda_n}} = \prod_{\lambda_n > \lambda_{crit}} \sqrt{\frac{\lambda_{crit}}{\lambda_n}}, \tag{S6}$$

with small corrections for eigenvalues $\lambda_n \approx \epsilon^2/\delta^2$. Since this result agrees with the "slab" argument given in the main text for hard walls, we see that hard ϵ-balls and hard δ-balls will have approximately the same amount of overlap as Gaussians.

Robustness, evolvability, and sloppiness

Derivation of chemotype evolvability

In the main text, we provide a formula for the "maximum fitness change among mutations of size δ in chemotype space"

$$e_c(\mathbf{F}, \boldsymbol{\theta}) = \sqrt{\mathbf{F}^T J J^T \mathbf{F}}\delta \tag{MT 3}$$

which we derive here using a Lagrange multiplier. To derive this, we use the definition of the chemotype evolvability as the maximum response $\mathbf{r} \cdot \mathbf{F}$ in R for moves in C of size $|\Delta\boldsymbol{\theta}| = \delta$:

$$e_c(\mathbf{F}, \boldsymbol{\theta}) = \max_{|\Delta\boldsymbol{\theta}|=\delta} (\mathbf{r} \cdot \mathbf{F}). \tag{S7}$$

Next, notice that

$$\mathbf{r} \cdot \mathbf{F} = (J\Delta\boldsymbol{\theta}) \cdot \mathbf{F} = \sum_i \sum_\alpha F_i J_{i\alpha} \Delta\theta_\alpha. \tag{S8}$$

We find the optimal $\Delta\boldsymbol{\theta}$ using a Lagrange multiplier Λ. With $(\Delta\boldsymbol{\theta})^2 = \delta^2$ as our constraint, we maximize

$$F_i J_{i\alpha} \Delta\theta_\alpha + \Lambda((\Delta\boldsymbol{\theta})^2 - \delta^2) = F_i J_{i\alpha} \Delta\theta_\alpha + \Lambda(\Delta\theta_\beta \Delta\theta_\beta - \delta^2) \tag{S9}$$

where we use the Einstein summation convention (summing over repeated indices). Differentiating with respect to $\Delta\theta_\alpha$, we can find the change $\Delta\theta^{max}$ giving the maximum response:

$$\Delta\theta^{max}_\alpha = \frac{F_j J_{j\alpha}}{2\Lambda} \tag{S10}$$

and hence

$$(\Delta\boldsymbol{\theta}^{max})^2 = \frac{F_i J_{i\alpha} J_{j\alpha} F_j}{4\Lambda^2} = \delta^2, \tag{S11}$$

which implies

$$\Lambda^2 = \frac{\mathbf{F}^T J J^T \mathbf{F}}{4\delta^2}. \tag{S12}$$

Therefore, the evolvability is:

$$\begin{aligned} e_c(\mathbf{F}, \boldsymbol{\theta}) &= F_i J_{i\alpha} \Delta\theta^{max}_\alpha = \frac{F_i J_{i\alpha} F_j J_{j\alpha}}{2\Lambda} \\ &= \frac{\mathbf{F}^T J J^T \mathbf{F}}{\sqrt{\mathbf{F}^T J J^T \mathbf{F}}}\,\delta = \sqrt{\mathbf{F}^T J J^T \mathbf{F}}\,\delta. \end{aligned} \tag{S13}$$

RMS dynatype evolvability

In Equation (5), to measure overall evolvability, we defined $E_c(\boldsymbol{\theta}_\alpha)$ as a root-mean-square (RMS) average over a uniform (hyper)spherical distribution of environmental forces $\mathbf{F}$ in dynatype space. We use the RMS $\sqrt{\langle e_c(\mathbf{F}, \boldsymbol{\theta}_\alpha)^2 \rangle}$ rather than the average $\langle e_c(\mathbf{F}, \theta_\alpha) \rangle$ because the RMS definition has an elegant result in terms of the eigenvalues λ_i of $J^T J$:

$$\begin{aligned} E_c(\boldsymbol{\theta}_\alpha)^2 &= \langle e_c(\mathbf{F}, \boldsymbol{\theta}_\alpha)^2 \rangle_{\mathbf{F}} = \langle \mathbf{F}^T J J^T \mathbf{F} \delta^2 \rangle_{\mathbf{F}} \\ &= \sum_i \frac{\int \lambda_i F_i^2 \, \mathrm{d}^N \mathbf{F}}{\int \mathrm{d}^N \mathbf{F}}\, \delta^2 \\ &= \sum_i \lambda_i \langle F_i^2 \rangle\, \delta^2 = \frac{\sum_i \lambda_i \langle \mathbf{F}^2 \rangle}{N}\, \delta^2 \\ &= \frac{Tr(J^T J) \langle \mathbf{F}^2 \rangle}{N}\, \delta^2 \approx \frac{Tr(H) \langle \mathbf{F}^2 \rangle}{N} \delta^2. \end{aligned} \tag{S14}$$

Therefore, the overall evolvability is directly related to the trace of the Hessian:

$$E_c(\boldsymbol{\theta}_\alpha) = \sqrt{\frac{Tr(H) \langle \mathbf{F}^2 \rangle}{N}}\, \delta. \tag{MT 5}$$

Our measures of robustness and evolvability depend upon our level of description, just as for Wagner's genotype and phenotype evolvabilities of RNA sequences (Ref. [8] of the main text). Our choice of an isotropic distribution of selective dynatype forces $\mathbf{F}$ is not intended as an accurate representation of actual selective forces at the phenotype level, but as an exhaustive study of all possible forces at the dynatype level of description.

Information about phenotypic selective pressures might suggest a different distribution of dynatype forces $\mathbf{F}$. Indeed, this formalism provides a mechanism for coupling maps across scales, which is an important unsolved problem. Just as the genotype-to-chemotype ($G \to C$) and chemotype-to-dynatype ($C \to D$) maps are many-to-one, so is the dynatype-to-phenotype map ($D \to P$). In the segment polarity model, for example, one might construe the phenotype as the steady-state pattern, whereas the dynatype will include information about all transient paths to that steady state. This is also closely analogous to measuring evolvability of RNA sequences by counting distinct folded structures (Ref. [8] of the main text), as many different structures may be equally nonfunctional at the higher level of biological phenotype. Ultimately, understanding the nature of the complex $D \to P$ maps will be required to estimate evolvability using more realistic distributions of selective dynatypic forces $\mathbf{F}$.

Figure 4: Evolvability and robustness in a sloppy system

When calculating the chemotype robustness R_c, we have a choice to make for the value of λ_{crit} (see Equation 2). This choice corresponds to setting the ratio of the size of acceptable changes in dynatype ϵ to the typical size of mutations δ in chemotype space: $\lambda_{crit} = \epsilon^2/\delta^2$.

Equivalently, λ_{crit} sets a cutoff between stiff and sloppy eigenvalues, since we assume that, in D space, the image of the δ-ball fully overlaps with the ϵ-ball in sloppy directions (with eigenvalues below λ_{crit}), and it extends far beyond the edge of the ϵ-ball in stiff directions (with eigenvalues above λ_{crit}).

In calculating R_c for the inset of Figure 4 in the main text, we chose λ_{crit} as the fourth stiffest eigenvalue of $J^T J$ at the best fit parameters. This matches with the idea that there are only a few stiff directions that appreciably constrain parameters in chemotype space: the eigenvalues are spaced by roughly factors of three (Figure 3), meaning mutations in sloppier directions in chemotype space quickly become irrelevant in dynatype space. The choice of λ_{crit} within a reasonable range (between, say, the second stiffest and eighth stiffest eigenvalue of $J^T J$) does not qualitatively change the plot of evolvability vs. robustness.